RESEARCH ARTICLE | FEBRUARY 14 2024

# Electron effective mass in GaN revisited: New insights from terahertz and mid-infrared optical Hall effect ⬤

Nerijus Armakavicius ✉ ⬤ ; Sean Knight ⬤ ; Philipp Kühne ⬤ ; Vallery Stanishev ⬤ ; Dat Q. Tran ⬤ ;
Steffen Richter ⬤ ; Alexis Papamichail ⬤ ; Megan Stokey ⬤ ; Preston Sorensen ⬤ ; Ufuk Kilic ⬤ ;
Mathias Schubert ⬤ ; Plamen P. Paskov ⬤ ; Vanya Darakchieva ⬤

Check for updates

View Online    Export Citation    CrossMark

# Electron effective mass in GaN revisited: New insights from terahertz and mid-infrared optical Hall effect ⒡

Nerijus Armakavicius,[1,2,3,a] Ⓘ Sean Knight,[1,2,3] Ⓘ Philipp Kühne,[1,2,3] Ⓘ Vallery Stanishev,[1,3] Ⓘ
Dat Q. Tran,[1,2,3] Ⓘ Steffen Richter,[2,3,4] Ⓘ Alexis Papamichail,[1,2] Ⓘ Megan Stokey,[5] Ⓘ Preston Sorensen,[5] Ⓘ
Ufuk Kilic,[5] Ⓘ Mathias Schubert,[2,4,5] Ⓘ Plamen P. Paskov,[1,2] Ⓘ and Vanya Darakchieva[1,2,3,4,b] Ⓘ

## AFFILIATIONS

[1] Department of Physics, Chemistry and Biology (IFM), Linköping University, 581 83 Linköping, Sweden
[2] Center for III-Nitride Technology, C3NiT–Janzén, Linköping University, 581 83 Linköping, Sweden
[3] Terahertz Materials Analysis Center (THeMAC), Linköping University, 581 83 Linköping, Sweden
[4] NanoLund and Solid State Physics, Lund University, 22100 Lund, Sweden
[5] Department of Electrical and Computer Engineering, University of Nebraska-Lincoln, Lincoln, Nebraska 68588, USA

[a] Author to whom correspondence should be addressed: nerijus.armakavicius@liu.se
[b] Electronic addresses: vanya.darakchieva@ftf.lth.se and vanya.darakchieva@liu.se

## ABSTRACT

Electron effective mass is a fundamental material parameter defining the free charge carrier transport properties, but it is very challenging to be experimentally determined at high temperatures relevant to device operation. In this work, we obtain the electron effective mass parameters in a Si-doped GaN bulk substrate and epitaxial layers from terahertz (THz) and mid-infrared (MIR) optical Hall effect (OHE) measurements in the temperature range of 38–340 K. The OHE data are analyzed using the well-accepted Drude model to account for the free charge carrier contributions. A strong temperature dependence of the electron effective mass parameter in both bulk and epitaxial GaN with values ranging from $(0.18 \pm 0.02)$ $m_0$ to $(0.34 \pm 0.01)$ $m_0$ at a low temperature (38 K) and room temperature, respectively, is obtained from the THz OHE analysis. The observed effective mass enhancement with temperature is evaluated and discussed in view of conduction band nonparabolicity, polaron effect, strain, and deviations from the classical Drude behavior. On the other hand, the electron effective mass parameter determined by MIR OHE is found to be temperature independent with a value of $(0.200 \pm 0.002)$ $m_0$. A possible explanation for the different findings from THz OHE and MIR OHE is proposed.

The electron effective mass in GaN is a key material parameter for understating charge transport mechanisms and for the design of GaN-based electronic devices. At very low temperatures (LT) (4–10 K), an effective mass of $(0.200–0.236)$ $m_0$ ($m_0$ is the free electron mass) has been experimentally determined by cyclotron resonance and far-infrared (FIR) spectroscopy of shallow donors in GaN.[1–3] However, due to the large broadening of the energy levels, these techniques are not applicable at higher temperatures, e.g., at room temperature (RT, 300 K) and above, which are much closer to device operation conditions.

Indirectly, mid-infrared (MIR) spectroscopy, which is sensitive to the coupling of plasmon and longitudinal optical (LO) phonons [i.e., to the longitudinal phonon–plasmon (LPP) modes], in combination with electrical Hall measurements, permits obtaining the electron effective mass parameter at higher temperatures.[4–6] In all these instances, free charge carrier contributions to the MIR optical response is analyzed using the classical Drude model. The RT effective mass of the electrons in GaN was determined by MIR reflectivity and electrical Hall effect measurements to be 0.22 $m_0$,[4] in good agreement with the LT results.[1–3] MIR spectroscopic ellipsometry

(MIR-SE) combined with electrical Hall measurements was also used to determine the anisotropy of the RT electron effective mass in GaN.[5,6] In a Si-doped GaN epitaxial layer with a free electron concentration of $N_e = 1 \times 10^{19}$ cm$^{-3}$, Kasic et al.[5] determined $m_\parallel = 0.228 \, m_0$ and $m_\perp = 0.237 \, m_0$ parallel and perpendicular to the c-axis, respectively. A slightly larger anisotropy has been reported for a-plane n-GaN layers with $N_e$ up to $1 \times 10^{19}$ cm$^{-3}$, with $m_\parallel = 0.216 \, m_0$ and $m_\perp = 0.239 \, m_0$.[6] Note that the electron effective mass and its anisotropy were found to be independent of the free electron concentration up to $N_e = 2 \times 10^{20}$ cm$^{-3}$.[6]

With the development of the optical Hall effect (OHE), which consists of performing generalized spectroscopic ellipsometry at long wavelengths in magnetic fields,[7,8] the determination of the electron effective mass and its anisotropy at LT to RT (and above) has become possible without the need to invoke additional electrical measurements. The OHE describes the external magnetic field-induced anisotropic charge displacement in materials when interacting with electromagnetic waves. For samples containing free charge carriers, the OHE causes detectable optical birefringence at longer wavelengths, where free charge carrier contribution to the optical response of the material is significant and can be measured by generalized spectroscopic ellipsometry. The free charge carrier sign, concentration, mobility, and effective mass parameters can be extracted from the experimental OHE data employing optical model-based analysis using the well-accepted Drude model to account for the free charge carrier contributions to the dielectric function.[8] Utilizing MIR and far-infrared (FIR) OHE measurements, the electron effective mass parameters and their anisotropy at RT in InN epitaxial layers ($m_\perp = 0.050 \, m_0$ and $m_\parallel = 0.037 \, m_0$),[9] In$_{0.33}$Ga$_{0.67}$N layers ($m_\perp \approx m_\parallel = 0.204 \, m_0$),[10] Al$_{0.72}$Ga$_{0.28}$N layers ($m_\perp \approx m_\parallel = 0.336 \, m_0$),[11] Al$_{0.79}$Ga$_{0.21}$N layers ($m_\perp \approx m_\parallel = 0.338 \, m_0$),[12] and bulk $\beta$-Ga$_2$O$_3$ ($m_e = (0.276-0.311) \, m_0$)[13] have been determined.

Previously, we have reported a strong temperature dependence of the electron effective mass parameter associated with the two-dimensional electron gas (2DEG) in AlGaN/GaN high electron mobility transistor (HEMT) structures determined by OHE in the terahertz (THz) domain.[14–16] The 2DEG effective mass parameter was found to be $0.22 \, m_0$ at temperatures up to 100 K, while at RT, an increase by ~50% was found. The observed effective mass enhancement was attributed to the temperature-induced delocalization of the electron wave function and penetration into the barrier layer having a higher effective mass parameter. However, such a high increase cannot be fully explained by electron wave-function hybridization due to the barrier layer material.[17,18] Similar results, consistent with our findings of significantly enhanced

2DEG effective mass, have been obtained by THz time-domain spectroscopy.[19–21] The observed increase in the electron effective mass parameter at THz frequencies indicates that additional phenomena in charge transport at higher temperatures may take place and raise the question of whether such an enhancement can occur for three-dimensional electrons in bulk GaN as well. This is vital to understand since electron effective mass may be the limiting factor on mobility and will impact the design and optimization of electronic devices operating at high frequencies and temperatures. However, no experimental results for the bulk electron effective mass parameter in GaN at THz frequencies and at temperatures above 100 K exist. So far, all the reports on the electron effective mass in bulk GaN at temperatures above 200 K have been based on the analysis of LPP modes determined by infrared spectroscopy or MIR-SE, which required additional electrical Hall measurements to be invoked.[4,5]

In this work, we determine the electron effective mass parameters in GaN bulk material and epitaxial layers doped with Si using THz and MIR OHE in the temperature range from 38 to 340 K. The classical Drude model, augmented to account for the effect of the magnetic field, is employed for the analysis of the OHE data. As a result, an electron effective mass parameter of $0.20 \, m_0$ is determined from MIR OHE and found to be the same at LT (60 K) and RT. On the other hand, the electron effective mass obtained by THz OHE shows a strong increase with increasing temperature, with $(0.20 \pm 0.02) \, m_0$ and $(0.34 \pm 0.01) \, m_0$ at LT (60 K) and RT, respectively. Different mechanisms that could contribute to the observed enhancement at THz frequencies are discussed, and a potential explanation for the differences from the MIR OHE results is proposed.

Three different GaN samples were studied: (i) sample A—Si-doped ($1 \times 10^{17}$ cm$^{-3}$) GaN substrate with a thickness of 500 $\mu$m (MSE Supplies), (ii) sample B—Si-doped ($5 \times 10^{17}$ cm$^{-3}$) 1-$\mu$m-thick GaN epitaxial layer, and (iii) sample C—Si-doped ($5 \times 10^{18}$ cm$^{-3}$) 1.5-$\mu$m-thick GaN epitaxial layer (Table I). The provided Si concentrations corresponded to the nominal doping values. The GaN substrate was fabricated by hydride vapor phase epitaxy, while the epitaxial layers were grown by hot-wall metalorganic chemical vapor deposition (MOCVD) on semi-insulating (SI) 4H–SiC(0001) substrates using AlN nucleation layers.[22,23]

Cavity-enhanced THz OHE[24] and MIR OHE measurements were employed to determine the free charge carrier properties using in-house-built THz[16] and MIR[25] ellipsometry setups operating in 300–500 and 600–1000 GHz, and 350–7900 cm$^{-1}$ (10.5–236.8 THz) ranges, respectively. The actual experimental spectral ranges used in the analysis were limited by low signal intensities at the detector,

**TABLE I.** Summary of the GaN samples and conditions of the optical Hall effect measurements.

| Sample | Description | [Si] (cm$^{-3}$) | Temperature range (K) | Magnetic field (T) | Spectral range |
|---|---|---|---|---|---|
| A | GaN substrate | $1 \times 10^{17}$ | 38–340 | 0, ±8 | THz:770–960 GHz |
| B | 1 $\mu$m GaN epitaxial layer | $5 \times 10^{17}$ | 86–300 | 0, ±8 | THz:340–1000 GHz |
| C | 1.5 $\mu$m GaN epitaxial layer | $5 \times 10^{18}$ | 60–300 | 0, ±6 | MIR:300–1700 cm$^{-1}$ |

20 March 2024 18:35:33

resulting in low signal-to-noise ratios, and sensitivity to the OHE at different temperatures. The measurements were performed in the Mueller matrix ellipsometry mode,[26] which provides access to the magneto-optic anisotropy of the samples (OHE). The THz and MIR ellipsometers operate in a polarizer-sample-rotating analyzer arrangement and provide access to the $3 \times 3$ upper left block ($M_{ij}/M_{11}$, where $i, j = 1, 2, 3$) of the $4 \times 4$ Mueller matrix ($M_{ij}/M_{11}$, where $i, j = 1, 2, 3, 4$). The Mueller matrix is based on Stokes vectors formalism and describes the polarization state change of light upon interaction with the sample. If the sample is optically isotropic, the off-diagonal block elements ($M_{ij}$, where $ij = 13, 23, 31, 32$) are equal to zero. When optical anisotropy is present, conversion between polarization components (e.g., s- and p-polarization modes) causes the off-diagonal block elements to deviate from zero. In this work, the optical anisotropy is induced by the OHE. The samples were placed in a cryostat with superconducting magnets providing a magnetic field parallel to the incoming THz and MIR beams (angle of incidence 45°).[16,25] The experiments were performed at temperatures of 60 K and RT (300 K) for the MIR measurements and from 38 to 340 K for the THz OHE measurements. Different temperature ranges are reported for different samples due to limited sensitivity to the OHE at different temperatures. The sensitivity of our equipment to the OHE depends on various factors, such as signal intensity at the detector, electron density and mobility parameters, and sample transparency. At each temperature, the measurements were performed at zero field as well as at B = ±8 T for THz OHE and B = ±6 T for MIR OHE, respectively.

The THz and MIR OHE data were analyzed by employing stratified layer model calculations using the $4 \times 4$ transfer matrix method (Berreman-formalism),[27] in combination with the Levenberg–Marquardt algorithm and parameterized model dielectric functions.[8] The extracted error bars represent the 90% confidence intervals derived from the covariance matrix of the fit parameters. The data analysis was carried out using the WVase32TM software (J.A. Woollam Co. Inc.). The model for epitaxial GaN layers consists of a semi-infinite layer with the metal backside, an air gap with variable thickness for the backside cavity, a uniaxial layer with variable thickness for the 4H–SiC substrate with the AlN nucleation, and GaN epitaxial layers with fixed thicknesses as determined from visible–UV spectroscopic ellipsometry (RC2, J.A. Woollam Co. Inc.). The optical properties of the metal backside are modeled with the classical Drude dielectric function with a free charge carrier density of $10^{23}$ cm$^{-3}$, a mobility of 5 cm$^2$ V$^{-1}$ s$^{-1}$, and an effective mass equal to the free electron mass $m_0$, which results in a near-perfect mirror behavior. The index of refraction of the backside cavity containing air is set to $n = 1$. For in-plane and out-of-plane refractive indices of 4H–SiC, $n_\perp = 3.13$ and $n_\parallel = 3.20$, respectively, were used in the model. These values were obtained by measuring the optical response of a bare 4H–SiC substrate in the THz region at RT. Our analysis is only sensitive to the product of substrate thickness and refractive index parameters, which exhibit negligible variations within the used temperature ranges. Moreover, the magnitude of the field difference data is not affected by the substrate index of refraction.

The dielectric function tensor of GaN at long wavelengths consists of contributions from free electrons and optical phonons. The phonon contribution is implemented as described in Refs. 10 and 11. All phonon parameters as determined by MIR spectroscopic

ellipsometry are fixed during the OHE data analysis. The magnetic field dependent free charge carrier contribution to the dielectric function tensor $\varepsilon^{FC}(\omega)$ is described using the classical Drude formalism including the change induced by the Lorentz force,[8]

$$\varepsilon^{FC}(\omega) = \frac{\omega_p^2}{-\omega^2 I - i\omega\gamma + i\omega\omega_c \begin{pmatrix} 0 & -b_z & b_y \\ b_z & 0 & -b_x \\ -b_y & b_x & 0 \end{pmatrix}}, \quad (1)$$

where $I$ is the identity matrix and $b_x, b_y,$ and $b_z$ are the scalar components of magnetic field vector $\vec{B}$, where each component is the projection along $x$, $y$, and $z$, respectively. The parameters in Eq. (1) are the screened plasma frequency tensor $\omega_p = \sqrt{(Nq^2/\varepsilon_0\varepsilon_\infty m^*)}$, the plasma broadening tensor $\gamma = q/\mu m^*$, and the cyclotron frequency tensor $\omega_c = q|\vec{B}|/m^*$. These parameters depend on the free charge carrier properties, which include the effective mass parameter $m^*$, the free charge carrier concentration $N$, the mobility $\mu$, and the elementary electric charge $q$, where $m^*$ and $\mu$ are the diagonal second rank tensors. In addition, $\varepsilon_0$ is the vacuum permittivity. In the isotropic average approximation of the given tensors, its values are replaced by scalar quantities and the corresponding unit matrix. Bulk carriers studied in this work were treated isotropically with mobility and effective mass parameters being scalar quantities. The OHE model assumes that Hall mobility and conductivity mobility are equal. Therefore, they should be considered as isotropically averaged parameters. A significant anisotropy of electron properties would lead to deviation of the experimental and model datasets, but no such deviations have been observed, confirming that the isotropic treatment of free electrons serves as a good approximation.

THz OHE was measured in samples A and B (GaN substrate and GaN layer with [Si] = $5 \times 10^{17}$ cm$^{-3}$), while MIR OHE was measured in sample C (GaN layer with [Si] = $5 \times 10^{18}$ cm$^{-3}$). The nominal Si concentrations in the GaN samples were chosen intentionally in order to maximize the OHE in the respective spectral ranges. In the MIR range, OHE is measured via the LPP coupling, which is the main phenomenon providing insight into the charge carrier properties through the resulting frequency shift of the coupled LPP mode with respect to the uncoupled mode.[10–12] To reach the detectable shift of the LPP mode requires relatively high carrier concentrations, typically, above $\sim 10^{18}$ cm$^{-3}$. The THz range is well below the LO phonon frequencies; however, the OHE detection is enabled due to the higher Drude contribution to the dielectric function of GaN as compared to the MIR range. This effect is further strengthened by the cavity enhancement, enabled by Fabry–Perot oscillations within the transparent sample/void/metal-mirror system.[28] Note that samples with a relatively high carrier density (product of carrier concentration and thickness parameters) are opaque in the THz range, impeding the use of cavity enhancement. In addition, if the electron mobility is relatively low, the OHE signal may be too small to be detected at THz frequencies. This is the reason why we were not able to detect THz OHE signal for the GaN layer with [Si] = $5 \times 10^{18}$ cm$^{-3}$. The GaN substrate was also opaque to the THz radiation at most temperatures; however, it has a much higher carrier mobility, enabling THz-OHE measurements. Details

about the respective THz and MIR OHE measurements are summarized in Table I. A slightly lower carrier concentration for sample A could provide an even higher sensitivity to OHE in the THz range; however, such substrates were not available to the authors. The Si doping in sample B is optimal, providing sufficient carrier density and sample transparency for cavity enhancement.

Figures 1–3 depict the variable-temperature experimental and best-matched calculated THz and MIR OHE difference Mueller matrix element data $\Delta M_{ij} = M_{ij}(B) - M_{ij}(-B)$ for the three samples. The magnetic field direction and type of charge carriers determine the sign of the induced OHE signal in the off-diagonal-block Mueller matrix elements ($M_{ij}$, $ij = 13, 23, 31, 32$). Hence, the field difference spectra (between $\pm B$ fields data) contain only the OHE signatures. These Mueller matrix elements are proportional to the cyclotron frequency and provide the most sensitivity to the effective mass parameter. Without in-plane crystal structure anisotropy, OHE induces symmetric off-diagonal block elements ($M_{ij} = M_{ji}$ with $ij = 13, 23$ and $ji = 31, 32$). Any difference in the off-diagonal block elements from zero represents the magnetic field-induced OHE signatures. Non-conductive samples reveal no OHE signatures. In the case of a zero magnetic field, all off-diagonal block elements are zero within the measurement error. Meanwhile, the on-diagonal block elements ($M_{ij}$, $ij = 12, 21, 22, 33$) are mainly determined by the plasma frequency and broadening parameters. There is a slight effect of the magnetic field on the on-diagonal block elements, which does not depend on the direction of the field or carrier sign. For this reason, on-diagonal block elements are zero at the calculated difference spectra. Note that all data measured for a specific temperature at zero and $\pm B$ fields and the respective differences between datasets at two opposite magnetic field directions ($M_{ij}[B] - M_{ij}[-B]$) and datasets with and without field ($M_{ij}[\pm B] - M_{ij}[0]$) are fitted simultaneously in our analysis. The respective zero- and $\pm B$ field measured and best-match calculated Mueller matrix data for the three samples are provided in the supplementary material (Figs. S1–S9).
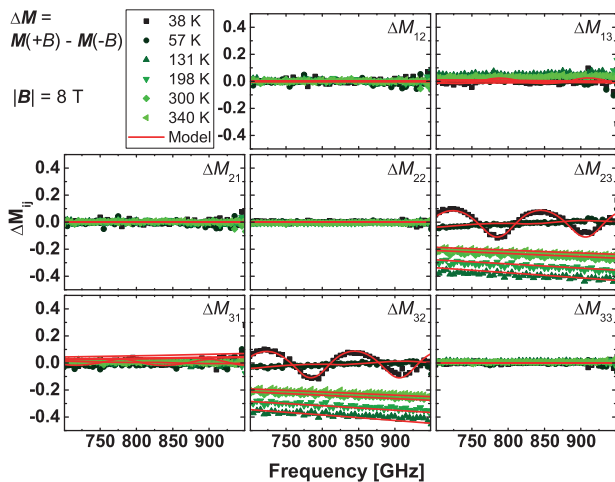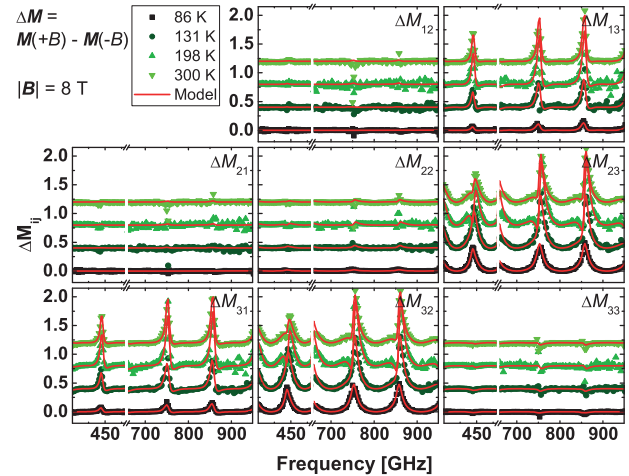


**FIG. 2.** Experimental and best-match calculated THz-OHE difference Mueller matrix spectra $[\Delta M = M(B) - M(-B)]$, $i, j = 1, 2, 3$, and B = $\pm 8$ T normalized to $M_{11}$ of sample B: GaN epitaxial layer (Si: $5 \times 10^{17}$ cm$^{-1}$). Data at different temperatures are shown. An offset of 0.4 is added to the datasets, starting from the 131 K dataset and continuing with subsequent sets as the temperature increases.

The THz OHE data for the GaN substrate (Fig. 1) represent a single reflection from the opaque medium for temperatures down to 57 K. The $M_{23}$ and $M_{32}$ elements strongly deviate from zero and display dispersion governed by the free electron properties via the OHE. As the temperature is reduced to 38 K, the GaN substrate becomes transparent as a result of free electron freeze-out (see the discussion below). The THz OHE data from sample B (GaN layer with [Si] = $5 \times 10^{17}$ cm$^{-3}$, Fig. 2) reveal OHE signatures following the Fabry–Perot oscillations pattern within the sample–air gap–mirror optical system, with the strongest OHE signatures in the
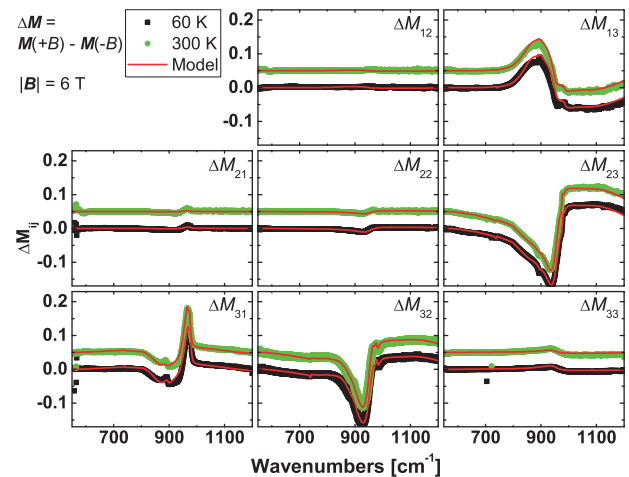


**FIG. 1.** Experimental and best-match calculated THz-OHE difference Mueller matrix spectra $[\Delta M = M(B) - M(-B)]$, $i, j = 1, 2, 3$, and B = $\pm 8$ T normalized to $M_{11}$ of sample A: GaN substrate (Si: $1 \times 10^{17}$ cm$^{-1}$). Data at different temperatures are shown.



**FIG. 3.** Experimental and best-match calculated MIR-OHE difference Mueller matrix spectra $[\Delta M = M(B) - M(-B)]$, $i, j = 1, 2, 3$, and B = $\pm 6$ T normalized to $M_{11}$ of sample C: GaN epitaxial layer (Si: $5 \times 10^{18}$ cm$^{-3}$). Data at 60 K and RT are shown. The offset of 0.05 is added to the RT data for a better visualization.

**TABLE II.** Results for the free electron concentration ($N$), isotropically averaged mobility ($\mu$), and effective mass parameter ($m^*$) at LT (60 K for samples A and C and 86 K for sample B) and RT (300 K) in GaN determined by THz and MIR OHE.

| Sample | $N$ (cm$^{-3}$) | | $\mu$ (cm$^2$ V$^{-1}$ s$^{-1}$) | | $m^*$ ($m_0$) | |
|---|---|---|---|---|---|---|
| | LT | RT | LT | RT | LT | RT |
| A | $(1.7 \pm 0.2) \times 10^{16}$ | $(1.8 \pm 0.3) \times 10^{17}$ | $538 \pm 63$ | $643 \pm 20$ | $0.18 \pm 0.02$ | $0.42 \pm 0.06$ |
| B | $(1.7 \pm 0.1) \times 10^{17}$ | $(4.1 \pm 0.1) \times 10^{17}$ | $347 \pm 10$ | $334 \pm 6$ | $0.20 \pm 0.02$ | $0.34 \pm 0.01$ |
| C | $(3.6 \pm 0.2) \times 10^{18}$ | $(3.7 \pm 0.1) \times 10^{18}$ | $133 \pm 1$ | $133 \pm 1$ | $0.200 \pm 0.001$ | $0.200 \pm 0.001$ |

spectral ranges where the reflectivity is the smallest. The lineshapes and amplitudes of these features are governed by the free electron properties. The MIR OHE data of sample C (GaN layer with [Si] = $5 \times 10^{18}$ cm$^{-3}$) represent the magnetic field-induced spectral OHE features determined by the coupled LPP mode, which shifts to higher wavenumbers with respect to the uncoupled longitudinal phonon mode with increasing electron density (Fig. 3).[10,11] The results on the best-matched model free charge carrier parameters at LT (60 K for samples A and C and 86 K for sample B) and RT are summarized in Table II, and the respective temperature dependencies are presented in Fig. 4.

The free electron concentration and electron mobility parameters obtained from the optical model with the best-match fit of the experimental OHE data at different temperatures are shown in Figs. 4(a) and 4(b). The free electron concentration in the GaN substrate (sample A) exhibits a strong temperature dependence due to thermal activation of the donor states. As a result, the free electron concentration increases from $1.6 \times 10^{16}$ cm$^{-3}$ (38 K) to $1.8 \times 10^{17}$ cm$^{-3}$ (300 K). On the other hand, the GaN layer with [Si] = $5 \times 10^{17}$ cm$^{-3}$ (sample B) demonstrates a relatively weak temperature dependence of the free electron concentration, which increases from $1.7 \times 10^{17}$ cm$^{-3}$ (86 K) to $4.1 \times 10^{17}$ cm$^{-3}$ (300 K). This indicates that most of the donors are already activated even at a temperature of 100 K. Finally, the free electron concentration in sample C (GaN layer with [Si] = $5 \times 10^{18}$ cm$^{-3}$) shows virtually the same electron concentrations of $3.6 \times 10^{18}$ cm$^{-3}$ and

$3.7 \times 10^{18}$ cm$^{-3}$ at 60 and 300 K, respectively. These results are in good agreement with the previously reported electrical Hall effect measurements showing that the free electron concentrations above $10^{18}$ cm$^{-3}$ are practically temperature independent,[29,30] suggesting that GaN becomes degenerate with the Fermi level in the conduction band for Si concentrations above ~$3 \times 10^{18}$ cm$^{-3}$.

The electron mobility parameters of sample A (GaN substrate) and sample B (GaN layer with [Si] = $5 \times 10^{17}$ cm$^{-3}$) exhibit a similar temperature dependence with the values being the highest in the 100–200 K temperature range (~1000 and ~400 cm$^2$ V$^{-1}$ s$^{-1}$, respectively) and then decreasing at lower and higher temperatures. These results are in good agreement with the previous report showing that for free electron concentrations below $10^{18}$ cm$^{-3}$, the mobility at LT decreases due to impurity scattering, while at higher temperatures, it is reduced as a result of optical phonon scattering.[30] Sample C (GaN layer with [Si] = $5 \times 10^{18}$ cm$^{-3}$) does not exhibit any significant change in the electron mobility parameter with the temperature as expected for the degenerately doped semiconductor.[31] Note that the free electron concentration and mobility parameters, determined by OHE as a function of temperature, are independently confirmed by electrical Hall effect measurements. Representative electrical Hall effect results for all the samples are shown in Figs. 4(a) and 4(b), revealing a good agreement with the respective OHE values, in particular the free electron concentration. Minor differences in the mobility parameters may be related to the different nature of the OHE and electrical Hall effect techniques, where the latter
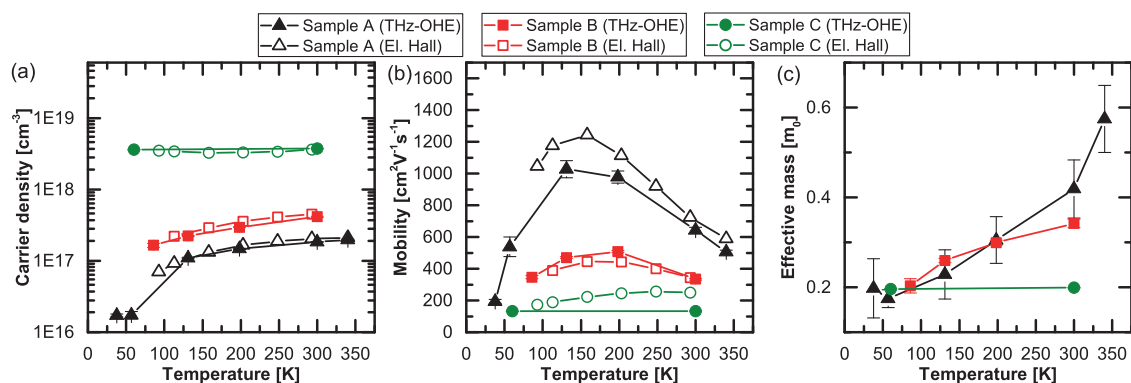
**FIG. 4.** The free electron concentration (a), the mobility (b), and the effective mass (c) determined by the THz OHE and MIR OHE measurements on the GaN substrate and GaN:Si epitaxial layers. The results for the electron density and mobility from the electrical Hall effect measurements are also included for comparison. The lines connecting the data points are a guide to the eye.

is influenced by the quality of the contacts and the assumption of conductive paths.[32]

The electron effective mass parameters as a function of temperature determined from the OHE data analysis are shown in Fig. 4(c). At temperatures below 100 K, the extracted electron effective mass parameters for all the samples are close to the literature value of $m_e = 0.22\ m_0$ (see Table II). For sample C (GaN layer [Si] = $5 \times 10^{18}\ \text{cm}^{-3}$), the MIR OHE measurements reveal a value of $m_e = 0.20\ m_0$ at both 50 and 300 K. The electron effective mass parameter in sample A (GaN substrate) and sample B (GaN epitaxial layer with [Si] = $5 \times 10^{18}\ \text{cm}^{-3}$) obtained from THz OHE measurements shows a strong temperature dependence with significant enhancement at temperatures above 100 K. The values obtained at 300 K, $m_e = 0.42\ m_0$ (sample A) and $m_e = 0.34\ m_0$ (sample B), are significantly larger than the reported GaN electron mass (experimentally and theoretically). We note that the error bar of the RT effective mass of sample A is significantly larger as compared to that of sample B since no cavity enhancement measurement scheme could be applied and a narrower frequency range was used in the former case. Therefore, the relatively high value of $m_e$ in sample A should be considered as a confirmation of the temperature-induced enhancement only, while the RT $m_e = 0.34\ m_0$ determined in sample B with a higher precision should be regarded as a more realistic quantitative estimate of the effect. Interestingly, this value is also very close to the RT effective mass determined by various THz techniques for 2DEG in AlGaN/GaN structures.[14–16,19,21] This indicates that the reported electron effective mass parameter enhancement at RT and THz frequencies may be associated with a general mechanism that is independent of the nature of the free charge carriers (2D vs 3D).

In principle, several prominent factors could potentially contribute to the enhancement of the electron mass in GaN: (i) conduction band nonparabolicity,[33] (ii) strain effects,[34] (iii) the presence of additional conductivity channels with heavier carriers, and (iv) electron–phonon coupling.[35]

Due to the large bandgap of GaN and the relatively low free electron concentration, the nonparabolicity effect is negligible for the samples studied here. Using the GaN nonparabolicity parameter[36] and the formalism given in Ref. 37, we can estimate the nonparabolicity-induced effective mass increase at RT of 0.1%, 0.2%, and 1.0% for samples A, B, and C, respectively. Strain effects can also be excluded since the GaN substrate (sample A) is virtually strain-free and the degree of strain in the GaN epitaxial layers is very small.[23] Different conductive channels are also unlikely to contribute to the observed increase in the electron effective mass. In the epitaxial layers, a potential two-dimensional hole gas (2DHG) may exist at the interface between the AlN nucleation layer and GaN. Holes have larger effective mass parameters of $1.4\ m_0$.[5] However, 2DHG, if existent, has a significantly lower mobility,[38] which in combination with the large hole effective mass results in negligible OHE being practically undetectable. Furthermore, despite the absence of interfaces for 2DHG formation, the GaN substrate (sample A) exhibits an effective mass enhancement with temperature.

The observed effective mass parameter enhancement is clearly temperature dependent, which suggests that it might be associated with free charge carrier interaction with optical phonons. GaN is a polar material, and significant electron–phonon coupling and polaron effects are expected. The polaron mass can be estimated by

$m_e^{pol} = m_e^b(1 + \alpha_e/6 + 0.0236\alpha_e^2)$, where $m_e^b$ is the bare electron mass and $\alpha_e$ is the Fröhlich coupling constant.[39] Using the Fröhlich coupling constant of 0.49,[1,40] we estimate an enhancement of 8% due to the polaron effect. This enhancement is significantly smaller than the observed increase in the RT electron effective mass determined by THz OHE.

Our findings clearly indicate that the electron effective mass parameter determined as a function of temperature has a very different behavior depending on whether THz OHE or MIR OHE is employed (Fig. 3). These results are supported by studies of AlGaN, InGaN, and InN layers by MIR-OHE and GaN by MIR spectroscopic ellipsometry at room temperature, where no effective mass enhancement beyond conduction band nonparabolicity effect was observed for various carrier concentration and mobility parameters.[5,9–11] In addition, our THz-OHE results reveal very similar room temperature effective mass parameters as in GaN-based HEMT structures, despite the differences in terms of electron confinement effects, concentration, and mobility parameters.[14–16,41] The temperature-dependent behavior of the phase shift introduced by a 2DEG in a GaAs/AlGaAs heterostructure at THz frequencies has very recently been reported,[42] suggesting that the phenomenon of enhanced electron effective mass parameter may not be limited to polar materials, such as GaN. Therefore, our results together with the previously published results point toward the importance of the probing frequency. In order to get further insight into this aspect, we consider in more detail the physical models used in the OHE data analysis [Eq. (1)].

The Drude formalism is consistent with the Boltzmann transport equation only when the relaxation time approximation (RTA) is used to simplify the collision integral by a single collision frequency.[43,44] However, if this approximation does not hold, the Drude description of the free charge carrier behavior may be insufficient. This may occur due to, for example, the interaction of the free electrons with the phonons.[45] Indeed, it is known that for certain metals and semiconductors, anomalies in the free charge carrier conductivity appear.[46–48] In such a case, the classical Drude model cannot provide a sufficient description and more general models are needed. A generalized Drude model not relying on RTA can be derived using projection operators.[44] One solution to this problem is to introduce a so-called memory function in the interpretation of the optical response of free charge carriers.[45,49,50] Using the memory function approach, the generalized Drude conductivity can be expressed in a form resembling the classical Drude expression, but with the effective mass $m^*$ and scattering time $\tau$ parameters replaced with the frequency- and temperature-dependent functions [$m^*(\omega, T)$ and $\tau(\omega, T)$, respectively] written in terms of complex memory function $M(\omega, T)$,[48]

$$m^*(\omega, T) = m^* \left(1 + \frac{Re(M[\omega, T])}{\omega}\right), \tag{2}$$

$$\tau(\omega, T) = \frac{1 + Re(M[\omega, T])/\omega}{Im(M[\omega, T])}. \tag{3}$$

Here, the function $m^*(\omega, T)$ is proportional to the effective mass $m^*$ and could be understood as the renormalized effective mass parameter. The function $\tau(\omega, T)$ becomes frequency- and temperature-dependent scattering time. When the RTA holds and the classical

picture provides a correct description of the free charge carrier response, the real part of the memory function $M_1(\omega, T)$ is equal to zero and the effective mass parameters in both the generalized and the classical Drude models are the same. If the classical Drude approach is used to extract the free charge carrier properties in situations when RTA does not hold, the deviations can be interpreted as renormalization of the effective mass parameters, which depends on frequency and temperature. Therefore, we suggest that a possible explanation for the observed enhancement of the electron effective mass parameter at high temperatures observed at terahertz frequencies and the lack of such enhancement in the MIR spectral range may be associated with deviation of the free charge carrier response from the classical Drude model. Such deviation can, for instance, be caused by a frequency-dependent scattering time, which becomes significant at temperatures above 100 K. This could have important implications for charge carrier transport in electronic devices operating at high temperatures and frequencies. It is worth noting that Korotyeyev *et al.* suggested that inelastic scattering of 2D electrons can lead to significant deviation of the high-frequency conductivity from the classical Drude model for the case of AlGaN/GaN heterostructures.[17] The proposed model can account for an increase in the 2DEG electron effective mass from 0.22 $m_0$ to 0.26 $m_0$ when temperature varies from 77 to 300 K.[17] Further development of this approach to describe the situation for 3D electrons should be pursued in order to elucidate whether such a mechanism is sufficient to explain the substantially larger enhancement of electron effective mass in GaN experimentally derived here. In addition, a comparison of theoretical calculations within the memory function approach with the experimental results presented here is of interest and should be further explored. Analytical derivation of the memory function for semiconductor materials has not been achieved so far. However, there are several approaches based on various assumptions proposed in the literature.[44,48,51]

In summary, we have determined the electron effective mass parameter in Si-doped GaN substrates and epitaxial layers using THz and MIR OHE techniques in the temperature range from 38 to 340 K. A well-accepted classical Drude description of the free charge carriers within the RTA, augmented for the effect of the magnetic field, was considered in describing the dielectric function of GaN. At LT, the electron effective mass is found to be ≈0.2 $m_0$ in all samples, which is in good agreement with the earlier results from cyclotron resonance techniques. The THz OHE data analysis reveals an increase in the electron effective mass parameter with temperatures in both bulk and epitaxial GaN with the RT value of $(0.34 \pm 0.03)$ $m_0$ (i.e., an increase of 55%). In contrast, the GaN electron effective mass parameters obtained from the MIR OHE are found to be the same $(0.200 \pm 0.002)$ $m_0$ at the low temperatures and room temperature. We have discussed the possible causes of the observed enhancement of the effective mass with temperature, including conduction band nonparabolicity, strain, and polaron effects, where all the contributions combined could account only for an ~9% increase. We suggest that the observed increase in the electron effective mass parameter beyond 9% (0.24 $m_0$) and the differences in the THz OHE and MIR OHE results may be caused by deviations of the free electron behavior from the classical Drude model. We speculate that the latter may be associated with a frequency-dependent scattering time. However, other effects could also contribute. This could have important implications for charge carrier transport at high temperatures

and frequencies, which calls for further theoretical and experimental studies to clarify the exact mechanisms.

The supplementary material contains the experimental and best-match model Mueller matrix elements spectra of the optical Hall effect at RT (Figs. S1–S12). It also includes the calculated dielectric function tensors with and without an external magnetic field, using the electron properties for sample A (GaN substrate) at RT (Figs. S13 and S14).

## AUTHOR DECLARATIONS

### Conflict of Interest

The authors have no conflicts to disclose.

### Author Contributions

**Nerijus Armakavicius**: Conceptualization (equal); Formal analysis (equal); Investigation (equal); Methodology (equal); Writing – original draft (equal); Writing – review & editing (equal). **Sean Knight**: Conceptualization (equal); Formal analysis (lead); Investigation (equal); Methodology (supporting); Writing – review & editing (supporting). **Philipp Kühne**: Investigation (supporting); Methodology (supporting); Validation (supporting). **Vallery Stanishev**: Methodology (supporting); Resources (supporting). **Dat Q. Tran**: Investigation (supporting). **Steffen Richter**: Methodology (supporting); Validation (supporting); Writing – review & editing (supporting). **Alexis Papamichail**: Investigation (supporting); Validation (supporting). **Megan Stokey**: Investigation (supporting). **Preston Sorensen**: Investigation (supporting). **Ufuk Kilic**: Investigation (supporting). **Mathias Schubert**: Funding acquisition (supporting); Methodology (equal); Resources (supporting); Validation (supporting); Writing – review & editing (supporting).

**Plamen P. Paskov**: Conceptualization (equal); Validation (supporting); Writing – review & editing (supporting). **Vanya Darakchieva**: Conceptualization (equal); Funding acquisition (equal); Investigation (equal); Methodology (equal); Resources (equal); Supervision (equal); Validation (equal); Writing – review & editing (equal).

## DATA AVAILABILITY

The data that support the findings of this study are available from the corresponding author upon reasonable request.

## REFERENCES

[1] M. Drechsler, D. M. Hofmann, B. K. Meyer, T. Detchprohm, H. Amano, and I. Akasaki, Jpn. J. Appl. Phys. **34**, L1178 (1995).

[2] B. K. Meyer, D. Volm, A. Graber, H. C. Alt, T. Detchprohm, A. Amano, and I. Akasaki, Solid State Commun. **95**, 597 (1995).

[3] A. M. Witowski, K. Pakuła, J. M. Baranowski, M. L. Sadowski, and P. Wyder, Appl. Phys. Lett. **75**, 4154 (1999).

[4] P. Perlin, E. Litwin-Staszewska, B. Suchanek, W. Knap, J. Camassel, T. Suski, R. Piotrzkowski, I. Grzegory, S. Porowski, E. Kaminska, and J. C. Chervin, Appl. Phys. Lett. **68**, 1114 (1996).

[5] A. Kasic, M. Schubert, S. Einfeldt, D. Hommel, and T. E. Tiwald, Phys. Rev. B **62**, 7365 (2000).

[6] M. Feneberg, K. Lange, C. Lidig, M. Wieneke, H. Witte, J. Bläsing, A. Dadgar, A. Krost, and R. Goldhahn, Appl. Phys. Lett. **103**, 232104 (2013).

[7] M. Schubert, T. Hofmann, and C. M. Herzinger, J. Opt. Soc. Am. A **20**, 347 (2003).

[8] M. Schubert, P. Kühne, V. Darakchieva, and T. Hofmann, J. Opt. Soc. Am. A **33**, 1553 (2016).

[9] T. Hofmann, V. Darakchieva, B. Monemar, H. Lu, W. Schaff, and M. Schubert, J. Electron. Mater. **37**, 611 (2008).

[10] N. Armakavicius, V. Stanishev, S. Knight, P. Kühne, M. Schubert, and V. Darakchieva, Appl. Phys. Lett. **112**, 082103 (2018).

[11] S. Schöche, P. Kühne, T. Hofmann, M. Schubert, D. Nilsson, A. Kakanakova-Georgieva, E. Janzén, and V. Darakchieva, Appl. Phys. Lett. **103**, 212107 (2013).

[12] S. Schöche, T. Hofmann, D. Nilsson, A. Kakanakova-Georgieva, E. Janzén, P. Kühne, K. Lorenz, M. Schubert, and V. Darakchieva, J. Appl. Phys. **121**, 205701 (2017).

[13] S. Knight, A. Mock, R. Korlacki, V. Darakchieva, B. Monemar, Y. Kumagai, K. Goto, M. Higashiwaki, and M. Schubert, Appl. Phys. Lett. **112**, 012103 (2018).

[14] T. Hofmann, P. Kühne, S. Schöche, J.-T. Chen, U. Forsberg, E. Janzén, N. Ben Sedrine, C. M. Herzinger, J. A. Woollam, M. Schubert, and V. Darakchieva, Appl. Phys. Lett. **101**, 192102 (2012).

[15] N. Armakavicius, J.-T. Chen, T. Hofmann, S. Knight, P. Kühne, D. Nilsson, U. Forsberg, E. Janzén, and V. Darakchieva, Phys. Status Solidi C **13**, 369 (2016).

[16] P. Kühne, N. Armakavicius, V. Stanishev, C. M. Herzinger, M. Schubert, and V. Darakchieva, IEEE Trans. Terahertz Sci. Technol. **8**, 257 (2018).

[17] V. V. Korotyeyev, V. A. Kochelap, V. V. Kaliuzhnyi, and A. E. Belyaev, Appl. Phys. Lett. **120**, 252103 (2022).

[18] P. Kühne, N. Armakavicius, A. Papamichail, D. Q. Tran, V. Stanishev, M. Schubert, P. P. Paskov, and V. Darakchieva, Appl. Phys. Lett. **120**, 253102 (2022).

[19] D. Pashnev, T. Kaplas, V. Korotyeyev, V. Janonis, A. Urbanowicz, J. Jorudas, and I. Kašalynas, Appl. Phys. Lett. **117**, 162101 (2020).

[20] R. B. Adamov, D. Pashnev, V. A. Shalygin, M. D. Moldavskaya, M. Y. Vinnichenko, V. Janonis, J. Jorudas, S. Tumėnas, P. Prystawko, M. Krysko, M. Sakowicz, and I. Kašalynas, Appl. Sci. **11**, 6053 (2021).

[21] D. Pashnev, V. V. Korotyeyev, J. Jorudas, A. Urbanowicz, P. Prystawko, V. Janonis, and I. Kašalynas, IEEE Trans. Electron Devices **69**, 3636 (2022).

[22] A. Papamichail, A. Kakanakova-Georgieva, E. O. Sveinbjörnsson, A. R. Persson, B. Hult, N. Rorsman, V. Stanishev, S. P. Le, P. O. Å. Persson, M. Nawaz, J. T. Chen, P. P. Paskov, and V. Darakchieva, J. Appl. Phys. **131**, 185704 (2022).

[23] R. Delgado Carrascon, S. Richter, M. Nawaz, P. P. Paskov, and V. Darakchieva, Cryst. Growth Des. **22**, 7021 (2022).

[24] S. Knight, S. Schöche, P. Kühne, T. Hofmann, V. Darakchieva, and M. Schubert, Rev. Sci. Instrum. **91**, 083903 (2020).

[25] P. Kühne, C. M. Herzinger, M. Schubert, J. A. Woollam, and T. Hofmann, Rev. Sci. Instrum. **85**, 071301 (2014).

[26] H. Fujiwara, *Spectroscopic Ellipsometry: Principles and Applications* (Wiley, 2007), pp. 81–146.

[27] M. Schubert, Phys. Rev. B **53**, 4265 (1996).

[28] S. Knight, S. Schöche, V. Darakchieva, P. Kühne, J.-F. Carlin, N. Grandjean, C. M. Herzinger, M. Schubert, and T. Hofmann, Opt. Lett. **40**, 2688 (2015).

[29] W. Götz, N. M. Johnson, C. Chen, H. Liu, C. Kuo, and W. Imler, Appl. Phys. Lett. **68**, 3144 (1996).

[30] Y. Arakawa, K. Ueno, H. Imabeppu, A. Kobayashi, J. Ohta, and H. Fujioka, Appl. Phys. Lett. **110**, 042103 (2017).

[31] M. L. Lovejoy, M. R. Melloch, and M. S. Lundstrom, Appl. Phys. Lett. **67**, 1101 (1995).

[32] We note that samples A and C have been measured by the electrical Hall effect at a later stage of the manuscript review process and certain slight changes of their free charge carrier properties with respect to the time of the OHE measurements (approximately a year earlier) could not be excluded.

[33] S. Syed, J. B. Heroux, Y. J. Wang, M. J. Manfra, R. J. Molnar, and H. L. Stormer, Appl. Phys. Lett. **83**, 4553 (2003).

[34] C. E. Dreyer, A. Janotti, and C. G. Van de Walle, Appl. Phys. Lett. **102**, 142105 (2013).

[35] S. A. McGill, K. Cao, W. B. Fowler, and G. G. DeLeo, Phys. Rev. B **57**, 8951 (1998).

[36] B. Arnaudov, T. Paskova, E. M. Goldys, S. Evtimova, and B. Monemar, Phys. Rev. B **64**, 045213 (2001).

[37] A. M. Kurakin, S. A. Vitusevich, S. V. Danylyuk, H. Hardtdegen, N. Klein, Z. Bougrioua, A. V. Naumov, and A. E. Belyaev, J. Appl. Phys. **105**, 073703 (2009).

[38] R. Chaudhuri, S. J. Bader, Z. Chen, D. A. Muller, H. G. Xing, and D. Jena, Science **365**, 1454 (2019).

[39] J. Rösler, Phys. Status Solidi B **25**, 311–316 (1968).

[40] A. V. Rodina, M. Dietrich, A. Göldner, L. Eckey, A. Hoffmann, A. L. Efros, M. Rosen, and B. K. Meyer, Phys. Rev. B **64**, 115204 (2001).

[41] S. Knight, S. Richter, A. Papamichail, P. Kühne, N. Armakavicius, S. Guo, A. R. Persson, V. Stanishev, V. Rindert, P. O. A. Persson, P. P. Paskov, M. Schubert, and V. Darakchieva, J. Appl. Phys. **134**, 185701 (2023).

[42] K. R. Dzhikirba, A. Shuvaev, D. Khudaiberdiev, I. V. Kukushkin, and V. M. Muravev, Appl. Phys. Lett. **123**, 052104 (2023).

[43] P. Bhalla and N. Singh, Int. J. Mod. Phys. B **33**, 1950128 (2019).

[44] K. Kumari and N. Singh, Eur. J. Phys. **41**, 053001 (2020).

[45] W. Götze and P. Wölfle, Phys. Rev. B **6**, 1226 (1972).

[46] S. J. Youn, T. H. Rho, B. I. Min, and K. S. Kim, Phys. Status Solidi B **244**, 1354 (2007).

[47] N. P. Armitage, arXiv:0908.1126 [cond-mat.str-el] (2018).

[48] Z. Rukelj, Phys. Rev. B **102**, 205108 (2020).

[49] R. Zwanzig, Phys. Rev. **124**, 983 (1961).

[50] H. Mori, Prog. Theor. Phys. **33**, 423 (1965).

[51] I. Kupčić, Phys. Rev. B **95**, 035403 (2017).